Interband and intraband optical transitions in InAs nanocrystal quantum dots: A pseudopotential approach

Theerapong Puangmali, Marco Califano, and Paul Harrison
Institute of Microwaves and Photonics, School of Electronic and Electrical Engineering, University of Leeds, Leeds LS2 9JT, United Kingdom

(Received 13 June 2008; revised manuscript received 22 September 2008; published 4 December 2008)

An atomistic pseudopotential method is used to investigate the electronic and optical properties of spherical InAs nanocrystals. Our calculated interband (valence-to-conduction) absorption spectra reproduce the features observed experimentally both qualitatively and quantitatively. The results relative to intraband (valence-to-valence and conduction-to-conduction) absorption successfully reproduce the recently measured photoinduced absorption spectra, which had so far been addressed only qualitatively. They exclude the hypothesis of a thermal activation process between dot-interior-delocalized hole states to explain the temperature dependence observed experimentally. Furthermore, based on the agreement of our data with the experimental valence intersublevel transitions and the almost complete overlap of the latter with scanning tunneling microscopic (STM) measurements, we question the simplistic attribution of the observed STM peaks obtained for negative bias.

DOI: 10.1103/PhysRevB.78.245104 PACS number(s): 73.21.La, 73.22.−f, 72.80.Ey

I. INTRODUCTION

The evolution of the electronic structure of semiconductor nanocrystals (NCs) as a function of size manifests itself as the transition from the molecular to the solid-state regime. To date, a number of observations of atomic-like electronic states in semiconductor NCs have been reported.[1,2] In particular, InAs quantum dots (QDs) have been the subject of a large volume of experimental[2–5] and theoretical[6–13] work, as they provide a typical example of quantum-confined systems in the technologically important group of narrow-gap materials and exhibit a spectrum of interesting properties that can find a wide range of applications.

Experimentally it is possible to resolve up to about nine peaks in the interband absorption spectra of colloidal InAs dots.[3] However, despite the extensive investigations conducted over the past decade, the origin of some of the optical transitions is still unclear. There is therefore scope for the application of a more accurate theoretical treatment to try to improve our understanding of such features.

One of the most widely used theoretical approaches is the continuum-like $\mathbf{k}\cdot\mathbf{p}$ method.[6] Banin *et al.*[3] used an eight-band $\mathbf{k}\cdot\mathbf{p}$ approach to study the size dependence of the optical transitions in InAs nanocrystals. They found that the energy of the observed ground-state transition identified as the optically allowed transition between the valence-band (VB) maximum [(VBM) $1S_{3/2}$] and the conduction-band (CB) minimum [(CBM) $1S_{1/2}$] deviated substantially from the prediction of their model when the radius of the NCs was less than 20 Å. Furthermore the multiband effective-mass model used in Ref. 3 entirely missed the second optical transition and achieved a good agreement with experiment only for the observed *strong* transitions, whereas the agreement for the weaker peaks was less satisfactory. The authors speculated that the discrepancy found for the ground-state energy could have been due to an underestimate of the electron wave-function penetration into the barrier or to the oversimplified calculation of electron-hole Coulomb interaction in the smallest crystals, in which the dielectric constant was taken as the static dielectric constant of bulk.

Using a different parametrization for the eight-band effective-mass Hamiltonian, Zhu *et al.*[7] found instead that the envelope function of the ground hole state (VBM) in InAs spherical dots has *p* symmetry and that therefore the transition from this level to the CBM ($1S_{1/2}$) is optically forbidden. Their calculated absorption spectrum, however, misses completely the sixth experimental peak and adds one extra unseen transition between the observed fourth and fifth peaks.

Another broadly used method is the atomistic tight-binding (TB) model.[8–11] The advantage of this method is that it allows to study large systems easily as the atomistic detail is limited to a small basis set. Furthermore, the TB model provides a simple physical picture in terms of the atomic orbitals and it has proved to be highly successful. However, the correct fitting of the band structure sometimes proved difficult in the past for the TB approach,[14] which also lacks detailed information about the atomic features of the wave functions. Niquet *et al.*[10] applied this model to study single-particle (SP) tunneling in InAs NCs. Their calculated band-gap energy and the splitting between the two lowermost conduction-band states were in good agreement with the STM data of Ref. 2. However, the calculated splittings between the two uppermost valence-band levels were much lower than the experimental values obtained for negative bias and assigned[2] to the transition between VBM and VBM-1. The authors[10] attributed this disagreement to the complexity of the structure of the STM charging peaks and questioned the simple interpretation given in Ref. 2 in terms of pure single-hole tunneling, pointing out that the model used by Banin *et al.*[2] could not account for the multiplicity and splitting of the negative bias peaks.

By using a different TB parametrization, Lee *et al.*[8] found a better agreement between their calculated hole addition energy spacings and the STM measurements. However the agreement between their calculated position for the three

strongest absorption peaks as a function of NC size and the experimental data was less than ideal, especially for $R < 20$ Å.

No theoretical work has so far been published on the analysis and interpretation of the recent photoinduced absorption (PIA) measurements carried out by Krapf *et al.*[5]

In this work we apply the semiempirical pseudopotential method[15] (EPM) to study intraband and interband optical transitions in InAs NCs with radii ranging from 15 to 30 Å. This approach, which uses a superposition of non-self-consistent screened atomic pseudopotentials to represent the total potential of a system, is ideally suited for a comprehensive microscopic description of a nanostructure. It provides a detailed description of the carrier wave functions on the atomic scale but may require a larger set of basis states compared to the TB method. This method was previously applied by Williamson and Zunger[13] to investigate the electron-hole excitations in InAs NCs. However, unlike in the present work where pseudo-hydrogen atoms (ligand potentials) are used to saturate the dangling bonds on the NC surface with an "atom by atom" passivation procedure (see below), in Ref. 13 an "effective-medium" passivation was used, where the NCs were embedded in two different artificial barrier materials: one for valence-band calculations and one for the conduction band. This choice resulted in an inversion of the order of the uppermost valence-band states compared with the present study and an overestimate of the strength of some high-energy transitions compared with experiment. Furthermore the calculations of Ref. 13 found no counterpart for the weakly observed fourth peak and their agreement with experiment was generally not as good as it is found here. Compared to Ref. 13, moreover, we use a slightly improved InAs pseudopotential.[16]

We obtain a good agreement with the observed absorption spectra in both interband and intraband transitions. Our results confirm the suitability of our method for describing the origin of the optical transitions in a wide range of nanocrystal sizes from very small NCs, where $\mathbf{k}\cdot\mathbf{p}$ and TB methods break down, to large systems.

The paper is organized as follows. In Sec. II we give a brief description of the EPM calculation method. In Sec. III the single-particle states and the interpretation of the optical transitions in InAs nanocrystals are presented. Our calculated results are compared with three complementary experiments: (i) STM;[2] (ii) PIA,[5] and (iii) photoluminescence excitation (PLE).[3] STM probes individual electron (hole) levels by consecutively charging the nanocrystals with one electron (hole) at a time; PIA can directly probe energy sublevel quantization in both conduction and valence bands; PLE examines exciton levels by optically creating electron-hole pairs. Our calculations are also compared with the available results obtained with $\mathbf{k}\cdot\mathbf{p}$ and TB methods. Section IV contains a summary of this work.

II. METHOD

There are three main steps in our calculation of the optical properties of semiconductor nanocrystals: (i) the construction of the atomistic structure of the NC; (ii) the solution of the single-particle Hamiltonian; and (iii) the calculation of the many-body effects. First, an As-centered InAs spherical quantum dot with the zinc-blende structure (lattice constant $a=6.0584$ Å) is constructed by adding successive atomic layers up to a specific cut-off radius r_{cut}. Surface atoms with only one bond are systematically removed and the dangling bonds at the surface of the quantum dots are passivated by pseudo-hydrogen atoms[17] whose parameters (bond length and potential details) are determined using an automated method[18] based on the global optimization algorithm DIRECT.[19] The ligand potentials have a Gaussian form,

$$V(r) = \alpha e^{-(|r-R_p|/\sigma)^2}, \tag{1}$$

where R_p is the location of the passivant atoms, α and σ represent, respectively, the amplitude and width of the Gaussian potential. The distance between the passivant and the center of the passivated atom equals ηd_0, where d_0 is the bulk In-As bond length and $0<\eta<1$. This 12-parameter set (represented by α, σ, and η for each type of possible surface atom: cations with one and two dangling bonds and anions with one and two dangling bonds) is optimized on flat (001-, 110-, and 111-oriented slabs) and curved (dots) test structures. The measure of the quality of a passivation is the extent to which the lowermost n states in the conduction-band and uppermost m states in the valence band are *not* on the NC surface. To estimate this the wave functions squared are integrated across the interior of each test structure, which is a more stringent test than the simple consideration of the position of the eigenenergies relative to the gap. To ensure that our results did not depend on the choice of the passivation parameters, we selected four sets yielding comparable "passivation quality" and calculated the single-particle gap and the *s-p* energy splitting in both valence and conduction bands. We found the difference in the results to be negligible and selected the set with highest quality factor. We use $\eta=0.57$ and 0.70 for In atoms with one and two dangling bonds, respectively, and $\eta=0.25$ for As atoms with both one and two dangling bonds.

The effective radius of the quantum dot (R) is defined in terms of the total number of atoms (not including passivants) in the dot (N_{dot}) as $R=a(\gamma N_{\mathrm{dot}})^{1/3}$, where $\gamma=3/(32\pi)$ for the zinc-blende structure.

The SP states of a quantum dot (Fig. 1, left-hand side) are then obtained by solving the Schrödinger equation

$$\left[-\frac{1}{2}\nabla^2 + V(r) + V_{\mathrm{SO}}\right]\psi_i(r) = \varepsilon_i\psi_i(r), \tag{2}$$

where V_{SO} is the spin-orbit coupling term and the local potential $V(r)$ is obtained as a superposition of screened atomic pseudopotentials for atom species α,

$$V(r) = \sum_{n,\alpha} V_\alpha(|r - R_{n,\alpha}|). \tag{3}$$

Equation (2) is then solved by expanding the pseudopotential wave functions in a plane-wave basis set, using the *folded spectrum method*,[20] which provides selected near-edge eigensolutions without having to solve for deeper energy levels.

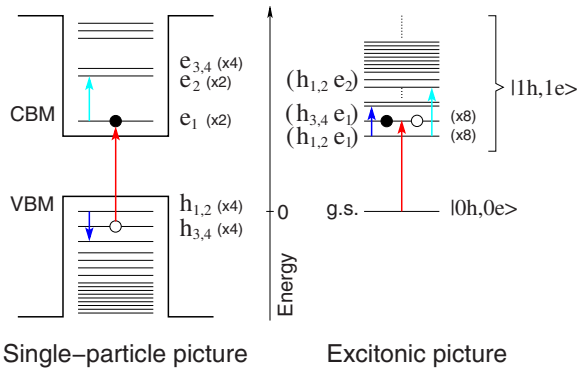

FIG. 1. (Color online) Schematics of energy levels and degeneracies in the single-particle (left-hand side) and excitonic (right-hand side) pictures. Single-particle levels are labeled as p_n, where $p=e,h$ is the charge carrier and n is the order of the level (increasing from 1 starting from the CBM upwards for e and from the VBM downwards for h). $\times d$ indicates the degeneracy (including spin). The zero of the energy is set arbitrarily at the position of the VBM. Single-exciton levels $|1h,1e\rangle$ are labeled according to the SP states from which they originate as (h_n,e_m). The zero of the energy is at the ground state $|0h,0e\rangle$ (i.e, the state with zero electrons and zero holes). In the case of InAs spherical NCs, the lowermost exciton manifold $(h_{1,2},e_1)$ originates from the SP states $h_{1,2}$ (VBM) and e_1 (CBM) and has therefore a total degeneracy of $4\times 2=8$. However exchange interaction splits it into a lower threefold-degenerate multiplet, a middle twofold-, and a higher threefold-degenerate multiplets, separated by energy gaps of the order of hundreds of μeV (not shown). We find very little configuration mixing in our InAs spherical NCs, with most excitons receiving a contribution $\geq 99\%$ from a single electron-hole pair (h_n,e_m). The arrows indicate intraband (short blue and cyan) and interband (long red) absorption processes.

We then calculate electron-hole direct and exchange Coulomb integrals[21] using the SP wave-function solution of Eq. (2). To evaluate the Coulomb integrals, we employ a size- and position-dependent microscopic dielectric function $\epsilon(r_1,r_2)$.[21]

Finally, we perform configuration-interaction (CI) calculations,[21] where the exciton wave functions $\Psi^{(a)}$ (where a denotes the exciton quantum numbers) are constructed as a linear combination of single substitution Slater determinants $\Phi_{v,c}$ composed of the antisymmetrized products of the SP wave functions $\psi_i(r)$ solutions of Eq. (2). We use the uppermost 80 states in the valence and lowermost 8 states in the conduction band for this expansion, yielding a total of 640 excitonic configurations.

A single-exciton level $|1h,1e\rangle$ can be labeled according to the SP states from which it originates as (h_n,e_m) (Fig. 1, right-hand side). In the absence of many-body interactions, the degeneracy of a level would simply be the product of the degeneracies of its composing SP states (i.e., $d_{h_n}\times d_{e_m}$) and its energy $E(h_n,e_m)=\varepsilon(e_m)-\varepsilon(h_n)$. However electron-hole Coulomb attraction lowers the energy of the exciton levels and exchange interaction splits them into multiplets (whose degeneracy depends on the material and shape of the NC) yielding the so-called excitonic fine structure. Furthermore due to configuration mixing, a further redshift occurs when different configurations (h_l,e_k) contribute to a (h_n,e_m)-derived exciton (for a step-by-step evolution from the single-particle approach to a full many-body treatment using configuration interaction, see Refs. 21 and 22).

Once the exciton wave functions have been obtained by diagonalizing the CI Hamiltonian, the dipole matrix elements for the optical interband absorption are calculated as

$$M^{(a)}=\sum_{v,c}A_{v,c}^{(a)}\langle\psi_v|\mathbf{r}|\psi_c\rangle, \tag{4}$$

where the coefficients $A_{v,c}^{(a)}$ are the eigenstates of the CI Hamiltonian. The optical-absorption spectrum is then calculated by

$$I(E)=\frac{1}{V}\sum_a |M^{(a)}|^2 e^{-(E-E^{(a)}/\Gamma)^2}, \tag{5}$$

where $E^{(a)}$ is the exciton energy and Γ represents an experimental line broadening. All absorption spectra (i.e., those relative to both intraband and interband transitions) in this work are calculated using excitonic states. However, as the single-particle picture is often more intuitive and given that the exciton states are found to be contributed to almost exclusively ($\geq 99\%$) by a single configuration, all absorption spectra presented in Sec. III are accompanied by the relevant calculated SP spectra illustrating the transitions between the single-particle states from which the different excitons involved originate. Intraband and interband transitions are represented schematically by colored arrows in Fig. 1.

III. RESULTS AND DISCUSSIONS

A. Single-particle states

Using the Hamiltonian described in Sec. II, the electron and hole energy levels and wave functions were calculated for InAs spherical dots with the effective radii $R=14.6$, 20, 21.7, 24.1, 25.8, 27.7, and 30 Å. In Fig. 2 we show the density of states (DOS) for the uppermost 40 states in the valence-band and lowermost ten states in the conduction band calculated for three representative NC sizes (the energies are relative to the VBM). The single-particle band gap exhibits the expected confinement-induced size dependence. Figure 3 shows the cross-sectional contour plots of the wave functions squared of the four uppermost (lowermost) valence (conduction) states on a (001) cut plane across the center of the spherical quantum dot with $R=14.6$ Å together with those relative to an elongated dot (rod) with the same small radius and an aspect ratio of length over diameter $L/D=1.4$. The single-particle levels in the conduction and valence bands are labeled according to Fig. 1. We find that for spherical quantum dots, the envelope functions of the first four electron states e_1–e_4 have mostly s, p, p, and p angular-momentum component, respectively, whereas the first two degenerate hole states h_1 and h_2, which have previously been identified as having prevalently s symmetry on the basis of $\mathbf{k}\cdot\mathbf{p}$ calculations,[2] have mostly p-like character and the next two degenerate states h_3 and h_4 have s-like character, in agreement with TB results.[8] In Ref. 2 the lowest CB level,

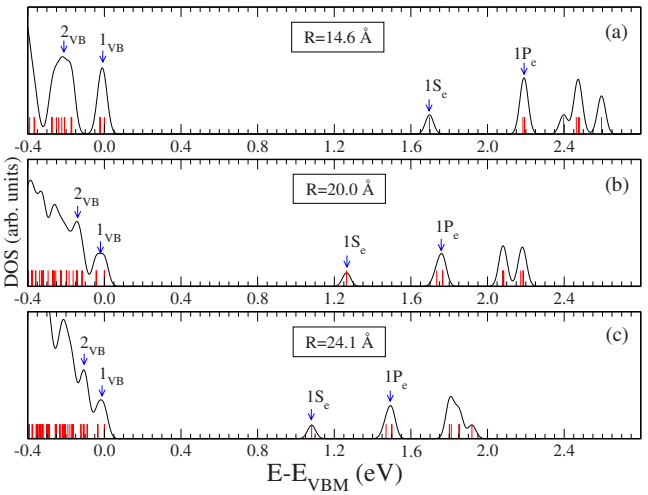

FIG. 2. (Color online) Density of states calculated for three InAs NCs with $R=14.6$, 20, and 24.1 Å using a broadening of 30 meV. The 40 (ten) uppermost (lowermost) states in the valence (conduction) band are included. The arrows indicate the positions of the DOS peaks which could correspond to the state assignment made in Ref. 2 (labels on the peaks).

$1S_e$, was found to be twofold degenerate and the next CB level, $1P_e$, was found to be sixfold degenerate. According to our calculations, spin-orbit coupling splits the sixfold-degenerate p-like state into one twofold- (e_2) and one fourfold- (e_3 and e_4) degenerate states (and the same is true for the higher Np states). Indeed, by setting $V_{SO}=0$ in Eq. (2), we recover the sixfold degeneracy for all the p states. In the valence band, the two highest levels 1_{VB} (h_1,h_2) and 2_{VB} (h_3,h_4) are fourfold degenerate.

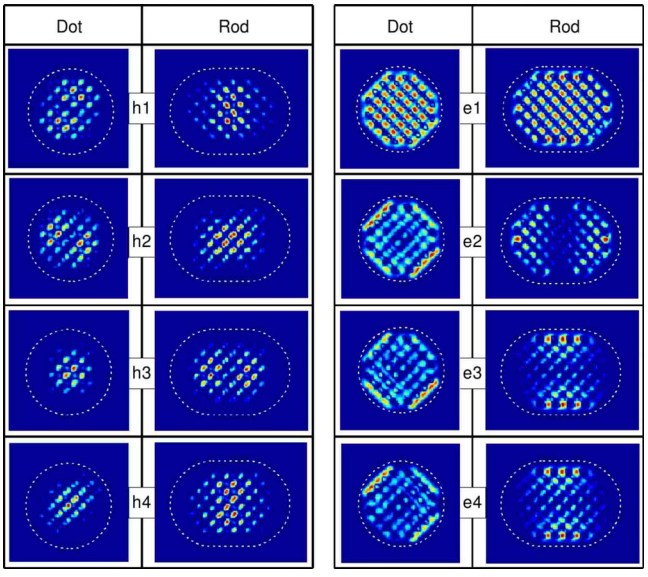

FIG. 3. (Color online) Comparison between the charge densities of the four uppermost (lowermost) states in the valence (conduction) band in InAs NCs with small radii of 14.6 Å and aspect ratio $L/D=1$ (dot) and 1.4 (rod). The cross-section contours are plotted on the (001) atomic plane with their intensity increasing from blue to red. The NC boundaries are represented by dashed lines.

In contrast to the order of the envelope functions of the spherical dot just described, we find a switching of levels in the valence band of elongated dots, where the first two hole states h_1 and h_2 have mostly s-like character whereas both h_3 and h_4 have prevalently p-like character. This effect can be explained in terms of reduced confinement. The bulk exciton Bohr radius (a_0) is a useful ruler for distinguishing between different quantum confinement regimes.[23,24] A strong confinement occurs once a critical dimension (d) of a semiconductor nanostructure is smaller than a_0, whereas a weak confinement is defined for cases where $d \gg a_0$. Significant length-dependent effects in slightly elongated dots are to be expected due to the large exciton Bohr radius in InAs nanocrystals (35 nm). We find[25] that the switching of the hole levels is both shape and size dependent, due to the interplay between quantum confinement and spin-orbit coupling, as previously observed:[8,24,26] the value of the aspect ratio at which s- and p-like hole levels cross increases fast with NC size from 1.4 for $R=14.6$ Å almost doubling to about 2.6 for the next size considered, $R=20$ Å. Therefore, the size and shape distributions should be carefully considered in the interpretation of experimental data.

The first detailed investigation on the electronic states in InAs nanocrystals was performed by Banin *et al.*[2] They used a colloidal technique to prepare InAs QDs that were nearly spherically shaped with radii ranging from 10 to 40 Å and performed scanning tunneling spectroscopy to identify the electronic states. Based on the correlation between the results of the latter and optical data,[3] they concluded that (i) the difference between the first two *groups* of STM peaks measured in the negative (positive) bias regime corresponded to the energy spacing between VBM and VBM-1 (CBM and CBM+1), and (ii) the topmost valence band (1_{VB}) had mixed s and p character, with prevalent s symmetry. It was not clear at that time whether there was an intrinsic mixing or degeneracy between different states having s and p character.[2] Our results show that the mixing (ii) is intrinsic (also see below) and that the hole states with (prevalent) s-like symmetry (the degenerate h_3, h_4 levels) are well separated in energy from those with (prevalent) p symmetry (the degenerate h_1, h_2 levels). In principle, the different ordering of the hole levels assumed in Ref. 2 could, however, has been due to the shape distribution in the experiment. It is plausible that the shape of the actual synthesized samples might not have been an ideal sphere. As discussed above, a slight elongation would have resulted in the switching of hole energy levels near the valence-band maximum for small NC sizes. The asymmetry associated with the underlying local Bloch states plays a significant role especially in small InAs structures, where it could yield a different type of energy sublevel hierarchy, particularly in the valence band, as previously found also in the $\mathbf{k}\cdot\mathbf{p}$ calculations of Efros and Rosen.[6] However our results show[25] that the absorption spectrum of a rod with $R > 14.6$ Å and with an aspect ratio large enough to exhibit an s-like VBM is substantially different from that of a dot and, most importantly, from the spectra measured experimentally in Ref. 3. We can therefore reject the hypothesis of an elongation in the experimental sample of such an extent as to cause the assumed inversion of symmetry in the uppermost valence-band states.

Previous pseudopotential calculations by Williamson and Zunger[13] also found a strongly mixed character, in terms of the angular-momentum components of the envelope functions, for the uppermost valence-band states in spherical NCs, but with a different proportion of *s* and *p* contributions compared to our results, yielding a prevalently *s*-like VBM in the size range considered ($12 \lesssim R \lesssim 21$ Å). In what follows we discuss the possible reasons for this disagreement. The ordering of electron and hole levels in *spherical* NCs is affected by different factors: (a) the dot size, (b) the strength of the spin-orbit (and both interband and intraband) coupling, and (c) the nature of the barrier that confines the carriers within the NC. In InAs NCs the level hierarchy has been shown[8,13] to depend on the dot size (a), due to the interplay between spin-orbit coupling (b) and quantum confinement, and to the different size scaling of the latter for different states. Strong couplings between heavy-hole, light-hole, and split-off bands, as well as between conduction and valence bands, have also been reported[8,13] to contribute to the complexity of the single-particle level structure, particularly in the valence band, in InAs NCs. The effect of different choices for the value of the confining potentials (infinite vs finite band offsets) has been well investigated in the literature[27] and has been shown to result, among other consequences, in large energy shifts and level crossings between single-particle states with different symmetries. As discussed by Reboredo and Zunger,[28] however, the physical nature of the barrier can influence the symmetry of the dot levels as well, without appreciably altering the excitonic transition energy. Furthermore, Singh and Kumar[29] recently showed that the mismatch of the value of the effective masses between barrier and dot material can have large effects on the NC energy levels, as a consequence of the BenDaniel-Duke boundary conditions.[30] The main difference between the calculations of Ref. 13 and the present work is precisely in the nature of the potential barrier (c). To simulate the effect of the organic ligands employed in experimental samples, here we use an "atom-by-atom" passivation achieved with hydrogenic-like potentials. In contrast, in Ref. 13 the same effect was obtained by passivating the NC surface using an "effective medium," i.e., an artificial barrier material represented by an atomic pseudopotential fitted to have (1) a larger band gap than InAs and (2) which produced a type I band alignment between dot and barrier. Such a barrier material however had also a set of effective masses associated with it, which was different from that of the dot. We believe that the value of this mass mismatch and the choice of the potential offset combined with the small energy separation between the *p* and *s* hole states (of the order of few tens of meV) played the main role in determining the different valence-band level hierarchy found in Ref. 13. It is important to stress that the two approaches model different *physical* barrier materials: for a realistic choice of the effective masses in the artificial barrier the approach used in Ref. 13 is perhaps better suited for core/shell structures (where the dot is surrounded by another semiconductor material), whereas the method used here is also applicable to organic-ligands-terminated NCs.

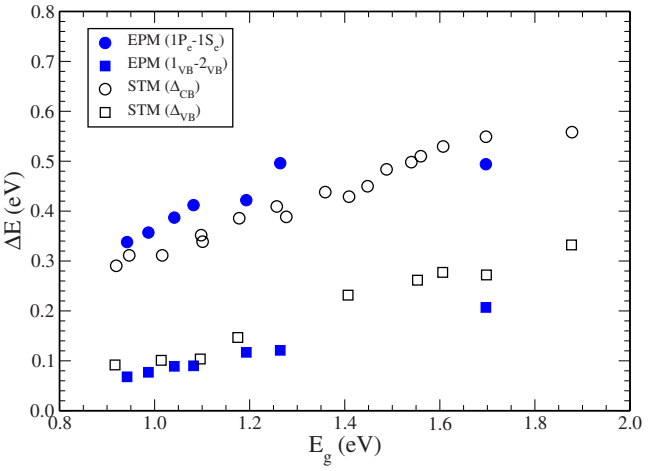

FIG. 4. (Color online) Comparison of the energy spacings between our calculated DOS peaks (blue solid symbols—for labeling see Fig. 2) and the measured STM (groups of) peaks [empty symbols, digitally extracted from Fig. 3b of Ref. 2], as a function of the single-particle energy gap.

As mentioned above, the simple interpretation (i) of Ref. 2, in terms of pure single-hole tunneling in the attribution of the STM peaks for negative bias, has been previously questioned by Niquet *et al.*,[10] who found a significative disagreement between their calculated energy spacing between the topmost two VB levels and the experimental data, and at the same time a good agreement for the same quantities in the CB (for $R > 20$ Å). A similar disagreement is found here with the VBM-(VBM-1) spacing ranging from 20 to 40 meV for the NC sizes considered here. However, if we assume that quasiparticle polarization self-energies are similar for different electron states,[31] we can compare the STM data with the spacings between our calculated DOS peaks. As it can be seen from Fig. 2, such spacings do not correspond to those between the two uppermost VB states but involve deeper hole levels. Our calculated DOS peak spacings are compared with those measured by STM in Fig. 4. From the fairly good agreement between theory and experiment, we conclude that (i) considering level-independent polarization self-energies is a reasonable approximation in InAs NCs, and (ii) the STM data relative to negative bias measurements cannot be simply explained in terms of the energy separation between the two uppermost VB levels.

Motivated by the close agreement between STM, PLE, and PIA experimental data found in Ref. 5, we therefore carried out a study of interband and intraband optical transitions in InAs NCs.

B. Intraband transitions

Figures 5(a) and 5(c) show, respectively, our calculated conduction- and valence-band (single-particle) energy levels for a 24.12-Å-radius dot. The corresponding (excitonic) intraband absorption spectrum at room temperature broadened with a Gaussian of widths $\Gamma = 5$ and 50 meV is shown in Fig. 5(b).

The small broadening allows all the transitions to be resolved, however, as such a resolution is not yet accessible

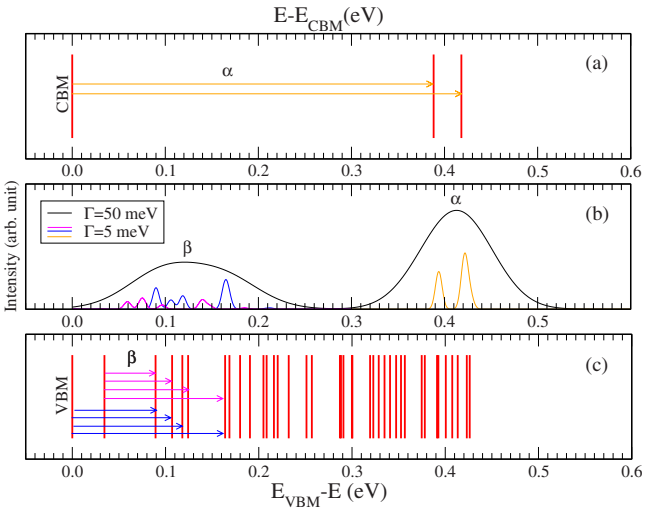

FIG. 5. (Color online) Calculated intraband transitions for InAs NCs with $R=24.1$ Å. (a) and (c) illustrate the intraband conduction-to-conduction (C-C) and valence-to-valence (V-V) single-particle transitions, respectively; (b) the calculated intraband (excitonic) absorption spectrum at room temperature with two different broadening lines ($\Gamma=5$ and 50 meV). For $\Gamma=5$ meV, the group of peaks β is decomposed into the different contributions from the two uppermost valence-band states: the features relative to transitions originating from the VBM (VBM-1) are marked with a blue (magenta) line in (b), according to the color code of the corresponding arrows in panel (c).

experimentally; we also use a larger value for Γ (estimated from the spectra reported in Ref. 5 for the same dot size), for a direct comparison with the observed features in the PIA spectra. The spectrum calculated with the largest broadening displays two well-defined absorption peaks: β (at 0.12 eV) and α (at 0.42 eV), each of which contains a group of smaller peaks that represent its "fine structure." These high-resolution peaks provide useful information for the interpretation of the observed temperature behavior. We have identified one group (β) to be related to inter-valence transitions while the other (α) is related to inter-conduction transitions. This feature agrees very well with the experimental results from photoinduced absorption spectroscopy.[5] However, although we agree with the assignment of the high-energy feature proposed by Krapf *et al.*,[5] our interpretation of the origins of the intravalence transitions differs from that suggested in Ref. 5.

The PIA measurements performed by Krapf *et al.*[5] evidenced two groups of intersublevel (ISL) transitions in colloidal InAs QDs. The first group, relative to conduction ISL (CISL) transitions, persists at all temperatures, while the second group, relative to valence ISL (VISL) transitions, is thermally activated and appears at temperatures above 100 K. The CISL feature was assigned to the $1S^e_{1/2} \rightarrow 1P^e_{3/2}$ ISL transition, between the ground sublevel for the conduction electron, and the first electron excited state. Our results confirm this level assignment, with the difference that—as mentioned before—in our calculations the $1p$ electron level is not sixfold degenerate but split by spin-orbit coupling into a lowermost twofold-degenerate state e_2 and an uppermost fourfold-degenerate state e_3, both of which contribute to the ISL absorption from the electron ground state e_1.

Krapf *et al.*[5] interpreted the observed VISL peak using a simple three-level system model with $|1h\rangle$, $|2h\rangle$, and $|3h\rangle$ denoting the ground, first-, and second-excited hole states, respectively. They concluded that the observed VISL transition was related to the $|2h\rangle \rightarrow |3h\rangle$ transition, corresponding to $1P^h_{3/2} \rightarrow 2S^h_{3/2}$, in $\mathbf{k}\cdot\mathbf{p}$ language. The transition $|1h\rangle \rightarrow |2h\rangle$ was explained in terms of thermal population, whereas the direct $|1h\rangle \rightarrow |3h\rangle$ transition was considered to be optically forbidden, corresponding to $1S^h_{3/2} \rightarrow 2S^h_{3/2}$.

In contrast to this simple picture, we find that the first feature (β) is composed of two overlapping groups of intraband absorption peaks [marked with blue and magenta lines in Fig. 5(b)], each arising from transitions originating from one of the two topmost fourfold-degenerate levels in the VB (VBM and VBM-1). Most importantly, both groups of peaks would be visible at low temperature, albeit with different intensities. (As a matter of fact, as shown in Fig. 5(c), the spectral features relative to transitions from the VBM are stronger than those arising from transitions originating from the VBM-1 state). Furthermore, as illustrated by the arrows in Fig. 5(c), the VISL transitions do not simply connect these two states to a single higher-energy hole state ($|3h\rangle$ in Ref. 5) but involve multiple higher excited hole levels. The fact that we predict transitions that originate from levels with different *prevalent* character (p and s for VBM and VBM-1, respectively) and end on the same final state (VBM-2, for example) is due to the intrinsic mixing of the envelope functions in terms of their angular-momentum components: as it can be clearly seen from Fig. 5(c), the transition VBM $\rightarrow$ VBM-2 is much stronger than VBM-1 $\rightarrow$ VBM-2, due to the similarity of the symmetry between the VBM and VBM-2 states.

Our calculated VISL transition energies are compared with PIA (and PLE) data in Fig. 6. From the excellent agreement obtained we draw the following conclusions: (i) the three-levels model used in Ref. 5 is inadequate to capture the complexity of intraband absorption in InAs NCs; (ii) the thermal activation effect observed experimentally, where the lowest energy PIA feature (attributed to VISL transitions) appeared above a temperature of 100 K, cannot be explained in terms of the thermal population of the VBM-1 ($|2h\rangle$) from a VBM state ($|1h\rangle$) optically inaccessible from the VBM-2 ($|3h\rangle$) level.

(i) Our model provides a more satisfactory interpretation of the PIA data because it is able to accurately describe the complex structure of the valence band of bulk InAs,[16] including the highly anisotropic heavy-hole effective masses and the strong spin-orbit coupling. In light of our results, the alternative hypothesis of a thermally activated VISL transition due to the presence of a shallow surface-localized state (as opposed to a thermal population process between dot-interior states), advanced in Ref. 5, seems a more likely explanation of the temperature dependence (ii) observed in the PIA experiments.

To obtain further confirmation of our interpretation of the observed optical features we next calculated the interband absorption spectra.

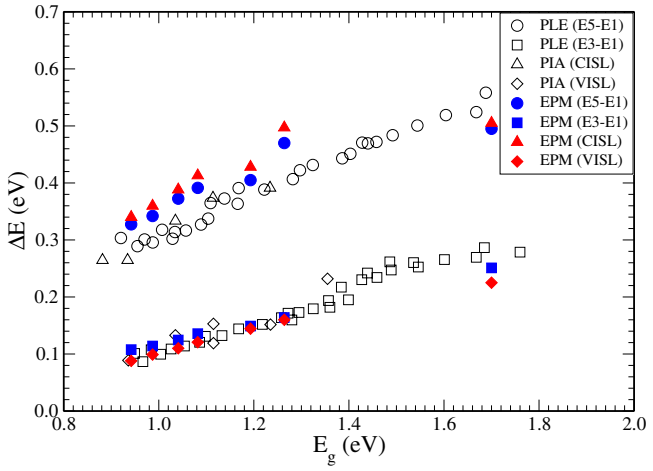

FIG. 6. (Color online) Comparison of our calculated intraband transition energies (red solid diamonds and triangles) and interband E5-E1 and E3-E1 energy spacings (blue solid circles and squares) with the valence and conduction intersublevel transition energies measured by PIA (empty diamonds and triangles, digitally extracted from Fig. 2 of Ref. 5) and PLE [empty circles and squares, digitally extracted from Fig. 3b of Ref. 2], see text, plotted as a function of the single-particle energy gap E_g (the same as in Fig. 4). The energies E1, E3, and E5 refer to the positions of the strongest peaks measured in absorption and are defined in Fig. 7 (and relative text).

C. Interband transitions

Figure 7 displays our calculated interband valence-to-conduction (V-C) absorption spectrum relative to a 24 Å radius NC and the corresponding transitions between single-particle energy levels, which represent the main contribution ($\geq$99%) to the different excitonic peaks. Using a line broadening of $\Gamma=10$ meV, we resolve several peaks each of which is associated with transitions having large oscillator

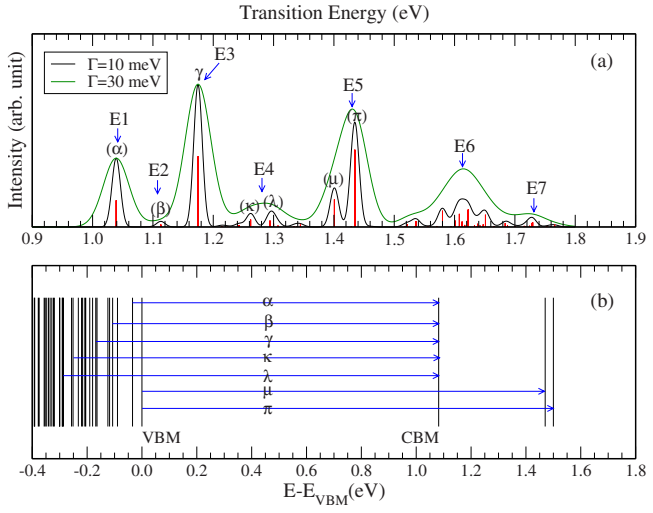

FIG. 7. (Color online) (a) Interband V-C absorption spectrum for an InAs nanocrystal with $R=24.1$ Å calculated with linewidths $\Gamma=0$ (red line), 10 (black line), and 30 meV (green line). The corresponding transitions between single-particle energy levels are shown in (b) with arrows. The lowest allowed transition (α) is the transition from VBM-1 to CBM.

strengths. To compare with PLE experiments,[3] we employ a line broadening of $\Gamma=30$ meV, whose effect is to wash out some of the weaker peaks, such as the β peak (peak E2 in the PLE experiment) and to merge other peaks, such as κ and λ into one single, broader feature (peak E4 in the PLE experiment). We therefore resolve three strong peaks α, γ, and π (corresponding to E1, E3, E5 in Ref. 3), with weaker features in between, in agreement with what is observed experimentally.[3]

A careful analysis of our results shows the following.

(a) Peak E1 corresponds to a transition with a strong intensity. In our calculation, the initial valence state associated with this transition is the second hole state (h_2=VBM-1) with mostly s-like character and the final conduction state is the electron ground state which has s-like character (see also Table I). It is interesting to note that our calculated transition between the ground hole state (h_1=VBM) and the ground electron state ($h_1 \rightarrow e_1$) has an oscillator strength which is typically about two orders of magnitude smaller than that between h_2 and e_1 and therefore cannot be observed. This finding is in accordance with the results of tight-binding calculations[8,9] but not with the $\mathbf{k}\cdot\mathbf{p}$ approach of Ref. 3.

(b) Peak E2 relates to a transition with such a weak intensity that it cannot be observed for all dot sizes in the PLE experiment. In our calculation this peak corresponds to the transition $h_4 \rightarrow e_1$ (a weak peak β in Fig. 7). Interestingly this feature was not predicted in the $\mathbf{k}\cdot\mathbf{p}$ approach of Ref. 3.

(c) Peak E3 has a strong intensity. The initial valence state associated with this peak is a fourfold-degenerate hole state (h_7) and the final conduction state is the doubly degenerate lowest energy electron state (e_1). In the $\mathbf{k}\cdot\mathbf{p}$ calculation, this is the $2S_{3/2} \rightarrow 1S_{1/2}$ transition and the $h_5 \rightarrow e_1$ (B2) transition in the tight-binding method.

(d) Peak E4 results from the merging of peaks κ and λ in Fig. 7 and has a weak intensity in good agreement with the weakly observed E4 in the PLE measurement. The initial single-particle states of these transitions are in the deeper levels in the valence band and the final state is the ground electron state (e_1). This corresponds to the $h_{16} \rightarrow e_1$ and $h_{19} \rightarrow e_1$ transitions in our calculation. This peak found no counterpart in either the $\mathbf{k}\cdot\mathbf{p}$ calculation of Ref. 3 or the EPM method of Ref. 13.

(e) Peak E5 is a very intense peak that is observed in all dot sizes. It relates to the transitions μ and π corresponding to $h_1 \rightarrow e_2$ and $h_1 \rightarrow e_3$. The initial state is the same for both transitions and has prevalently p-like character and both final states have mostly p-like character. In the $\mathbf{k}\cdot\mathbf{p}$ approach, these transitions are closest to the transitions $1P_{3/2} \rightarrow 1P_{3/2}$ and $1P_{3/2} \rightarrow 1P_{1/2}$. In the tight-binding method, this peak is assigned to the $h_1 \rightarrow e_2$ (B3) transition, where e_2 is sixfold degenerate.

By using 80 states in the valence band and eight in the conduction band, we calculate more than seven absorption peaks. However, as it can be seen from the multiple features below peak E6 in Fig. 7, the assignment of the highest of them in terms of single-particle transitions becomes increasingly complicated due to the large number of states involved. We compare our results with the experimental data[3] in Fig. 8.

Due to the fact that precise experimental size determinations are relatively difficult, a more compelling comparison

TABLE I. Comparison of the assignment of the first five peaks in the PLE measurement (Ref. 3) according to the current EPM, the tight-binding, and the $\mathbf{k}\cdot\mathbf{p}$ approaches. For the EPM calculation, the subscripts denote the order of different single-particle electron and hole energy levels (excluding degeneracy), whereas the numbers in the upper parenthesis denote the order of single-particle energy states including degeneracy (i.e., the first twofold-degenerate hole level is $h_1^{(1,2)}$, the next $h_2^{(3,4)}$, and so on). In the tight-binding method, the levels e_1 and e_2 are the first (twofold) and the second (sixfold) lowest electron levels, whereas the levels h_1 and h_2 are the first (fourfold) and the second (fourfold) lowest hole levels. The degeneracy mentioned in the TB approach includes spin as well. The first three strongest bright excitons in the tight-binding method are labeled as B1, B2, and B3. However, although other weaker peaks have been predicted to occur in Ref. 8, they have not been assigned to specific transitions. The notation for the electron and hole states in $\mathbf{k}\cdot\mathbf{p}$ method nQ_F, where n is the main quantum number, $Q=S,P,D,\ldots$, denotes the lowest angular momentum (L) in the envelope function and F is its total angular momentum. The second and fourth peaks have not been predicted in the approach of Ref 3.

Peak	EPM	Tight binding[a]	$\mathbf{k}\cdot\mathbf{p}$ [b]
E1	$h_2^{(3,4)}\rightarrow e_1^{(1)}$	$h_2\rightarrow e_1$ (B1)	$1S_{3/2}\rightarrow 1S_{1/2}$
E2	$h_4^{(7,8)}\rightarrow e_1^{(1)}$	Not assigned	Not predicted
E3	$h_7^{(11,12)}\rightarrow e_1^{(1)}$	$h_5\rightarrow e_1$ (B2)	$2S_{3/2}\rightarrow 1S_{1/2}$
E4	$h_{16}^{(25,26)}\rightarrow e_1^{(1)}$, $h_{19}^{(30)}\rightarrow e_1^{(1)}$	Not assigned	Not predicted
E5	$h_1^{(1,2)}\rightarrow e_2^{(2)}$, $h_1^{(1,2)}\rightarrow e_3^{(3,4)}$	$h_1\rightarrow e_2$ (B3)	$1P_{3/2}\rightarrow 1P_{3/2}$, $1P_{3/2}\rightarrow 1P_{1/2}$

[a]Reference 8.
[b]Reference 3.

with the PLE data emerges when the energies of higher transitions are plotted relative to the first bright-exciton energy (E1). However, as often the determination of the position of a peak and/or its experimental "visibility" are not trivial, we decided to show in Fig. 8(b) all peaks resolved using the smaller line broadening ($\Gamma=10$ meV), color coded corresponding to the broader peaks ($\Gamma=30$ meV) they contribute to. As a guide to the reader, the absorption peaks corresponding to the largest and smallest NC size studied in this work

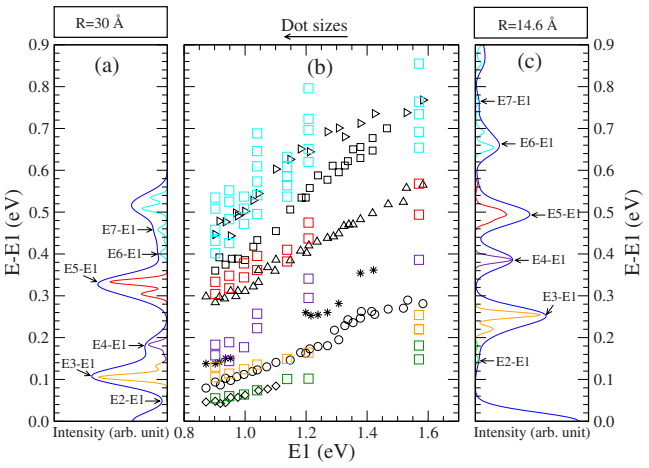

FIG. 8. (Color online) Calculated positions of the optical-absorption features, relative to the first strong absorption peak (E1), in InAs NCs with radii ranging from 14.6 to 30 Å. Panels (a) and (c) display the absorption spectra relative to E1 for the largest and smallest NCs, respectively, with linewidths Γ of 10 (ideal, colored line) and 30 meV (experimental-like, blue line): peaks with $\Gamma=10$ meV contributing to the same broad peak with $\Gamma=30$ meV have the same color. (b) Positions of all the absorption peaks calculated with $\Gamma=10$ meV (squares) relative to the first bright exciton (E1) versus E1 for InAs quantum dots with effective radii of 14.6, 20, 21.7, 24.1, 25.8, 27.7, and 30 Å, compared with PLE data (black symbols, digitally extracted from Fig. 4 of Ref. 3). The color coding corresponds to that used in panels (a) and (c).

(using both a large experimental-like broadening and a small ideal broadening) are also illustrated in Figs. 8(a) and 8(c) and color coded to identify the corresponding features in (b).

We find very good agreement with experiment for the spacings between the first four peaks and the band-edge exciton (E2-E1, E3-E1, and E4-E1) down to the smallest NC size (14.6 Å radius). This result is especially remarkable considering that some of these transitions are either not predicted at all[3,13] or have not been assigned[8] in previous theoretical studies. Since, as described above (see also Fig. 7), peaks 1–4 originate from transitions between different hole states and the electron ground state e_1, these results, together with the good agreement already found with the observed VISL transitions,[5] confirm the suitability of our model for the description of the valence-band structure and the band-gap energy in InAs NCs within a wide size range. The agreement obtained with the position of the fifth and sixth peaks is less ideal and reflects the slight overestimate of the level spacing in the conduction band we found for CISL transitions. The position of peak 7 is again in good agreement with observation.

Figure 9 shows the comparison of the exciton energies of the first three strongest absorption peaks, relative to the energy of the band-edge exciton, between the present model and the other theoretical frameworks ($\mathbf{k}\cdot\mathbf{p}$ calculations[3] and the tight-binding method[8]). A comparison of their assignment in terms of single-particle transitions according to our semiempirical pseudopotential calculation and the other theoretical methods is shown in Table I.

The energy spacing E3-E1 calculated with our approach shows a better agreement with experiment than the results of both $\mathbf{k}\cdot\mathbf{p}$ (Ref. 3) and tight-binding[8] calculations. This supports our claim that our model provides an accurate description of the complex structure of the valence band, correctly accounting for the anisotropy of the heavy-hole effective masses[16] and the strong coupling among heavy-hole, light-hole, and spin-split bands, which play an important role in determining the overall single-particle level spectrum. Surprisingly, however, the $\mathbf{k}\cdot\mathbf{p}$ and tight-binding methods pro-

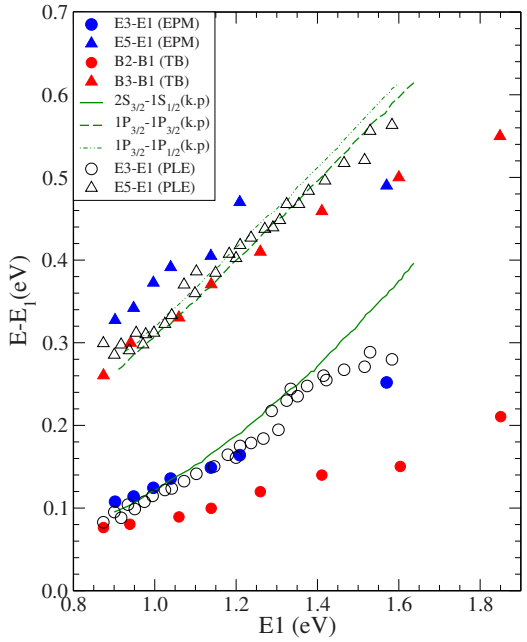

FIG. 9. (Color online) First three strong-exciton energies relative to the lowest bright-exciton energy plotted with respect to the lowest bright exciton position. In addition to the comparison with PLE data (digitally extracted from Fig. 4 of Ref. 3), our results are compared with the results of the tight-binding method (Ref. 8) as well as the multiband effective-mass model (Ref. 3).

vide a better description of the electron levels in the less complex conduction band, as illustrated by the comparison with the PLE data for the energy spacing E5-E1 reported in Fig. 9. A possible reason for this can be found in the "fine structure" of our calculated peaks: as shown in Fig. 7 our fifth peak is actually composed of two peaks μ and π relative to transitions from the VBM to the two spin-orbit split p-like electronic states e_2 and e_3, respectively. In our calculations the second of those peaks (π) is the strongest and therefore the position of E5 is blue shifted toward it. If peak μ were the strongest, the position of E5 could shift to the red by as much as the e_2-e_3 splitting, which is of the order of a few meV for the smallest NC considered here, increasing to a few tens of meV depending on the NC size. This would bring our results in closer agreement with experiment, as it is the case for the 14.6-Å-radius NC, where such splitting is small. A similar argument applies to our calculated PIA spectra. In contrast, in neither $\mathbf{k}\cdot\mathbf{p}$ nor tight-binding approaches, the p-like electron state is split and therefore their calculated E5-E1 energy separation is not affected by the magnitude of this splitting.

Another explanation could be provided by the shape of the experimental samples: elongated NCs exhibit substantially smaller spacings between s and p levels in the conduction band without showing significant decreases in the separation between the same states in the valence band, compared to spherical structures.[25] We previously excluded elongation as an explanation for the different level ordering at the top of the valence band assumed in Ref. 2, on the basis that the crossover between s and p states would require too large values of the aspect ratio, which would result in large morphological changes in the absorption spectra, incompatible with observation. However, slight elongations in the NCs resulting in aspect ratios small enough not to change appreciably the shape of the absorption spectra (nor the level hierarchy in the valence band) could account for the deviation from experiment of all our results involving the spacing between conduction-band states.

IV. CONCLUSIONS

We applied the pseudopotential method to investigate the optical properties of InAs NCs with $14.6<R<30$ Å. Our accurate description of the complex structure of the valence band allows us to successfully explain the low-energy features observed in recent PIA measurements. Based on this result we rejected the simplistic interpretation of such features in terms of a three-level model and the hypothesis of a thermal population process between hole states delocalized in the dot interior advanced in Ref. 5 to explain the experimentally observed temperature dependence of the low-energy PIA feature. We also questioned, as previously done by Niquet *et al.*[10] based on the results of TB calculations, the explanation of the results of STM experiments in the negative bias regime in terms of the energy separation between the two uppermost valence-band levels VBM and VBM-1, suggesting instead an interpretation based on the separation between the peaks in our calculated density of states.

Our calculated interband absorption spectral features reproduce those observed experimentally, showing three strong peaks (1, 3, and 5) separated by weaker features. We achieve a good agreement for the energy position of the first four peaks and the seventh down to NCs with $R=14.6$ Å. This result is especially remarkable considering that (i) some of these transitions were either not predicted at all[3,13] or were not assigned[8] in previous theoretical studies; (ii) the size range considered here includes very small NCs, i.e., a confinement regime where all other theoretical approaches break down. The agreement with the position of peaks 5 and 6 (and the, closely related, position of our calculated CISL peaks) is less ideal but still reasonable. We attribute this result either to a "fine-structure" effect in the conduction band, where strong spin-orbit coupling induces a sizeable splitting in the otherwise sixfold-degenerate first-excited state or to a slight elongation in the experimental samples, which would result in a decreased spacing between conduction-band energy levels.

In summary, the pseudopotential method provides an accurate description of the complex energy-level structure (especially in the valence band) of InAs NCs and presents itself as a suitable approach to explain many experimental features observed in both intraband and interband optical absorption spectra.

ACKNOWLEDGMENTS

We are grateful to Alex Zunger for insightful discussions and for granting us permission to use the NanoPSE computational package developed at the National Renewable Energy Laboratory (Golden, CO, U.S.A.) for all the calculations

performed here. We would like to thank Peter Graf for kindly providing the code used for the NC passivation and for his precious help and advice in the passivation procedure. T.P. thanks the Thai government for financial support. M.C. gratefully acknowledges the Royal Society for financial support under the URF scheme.

[1] A. P. Alivisatos, Science **271**, 933 (1996).
[2] U. Banin, Y. W. Cao, D. Katz, and O. Millo, Nature (London) **400**, 542 (1999).
[3] U. Banin, C. J. Lee, A. A. Guzelian, A. V. Kadavanich, A. Alivisatos, W. Jaskolski, G. W. B. A. L. Efros, and M. Rosen, J. Chem. Phys. **109**, 2306 (1998).
[4] U. Banin and O. Millo, Annu. Rev. Phys. Chem. **54**, 465 (2003).
[5] D. Krapf, S. H. Kan, U. Banin, O. Millo, and A. Saar, Phys. Rev. B **69**, 073301 (2004).
[6] A. L. Efros and M. Rosen, Annu. Rev. Mater. Sci. **30**, 475 (2000).
[7] Y. H. Zhu, X. W. Zhang, and J. B. Xia, Phys. Rev. B **73**, 165326 (2006).
[8] S. Lee, J. Kim, L. Jönsson, J. W. Wilkins, G. W. Bryant, and G. Klimeck, Phys. Rev. B **66**, 235307 (2002).
[9] S. Lee, L. Jönsson, J. W. Wilkins, G. W. Bryant, and G. Klimeck, Phys. Rev. B **63**, 195318 (2001).
[10] Y. M. Niquet, C. Delerue, M. Lannoo, and G. Allan, Phys. Rev. B **64**, 113305 (2001).
[11] Y. M. Niquet, C. Delerue, G. Allan, and M. Lannoo, Phys. Rev. B **65**, 165334 (2002).
[12] A. Mizel and M. Cohen, Solid State Commun. **104**, 401 (1997).
[13] A. J. Williamson and A. Zunger, Phys. Rev. B **61**, 1978 (2000).
[14] G. Allan and C. Delerue, Phys. Rev. B **70**, 245321 (2004).
[15] L.-W. Wang and A. Zunger, Phys. Rev. B **51**, 17398 (1995).
[16] R. Magri and A. Zunger, Phys. Rev. B **65**, 165302 (2002).
[17] L.-W. Wang and A. Zunger, Phys. Rev. B **53**, 9579 (1996).
[18] P. A. Graf, K. Kim, W. B. Jones, and L. W. Wang, J. Comput. Phys. **224**, 824 (2007).
[19] D. R. Jones, C. D. Perttunen, and B. E. Stuckman, J. Optim. Theory Appl. **79**, 157 (1993).
[20] L.-W. Wang and A. Zunger, J. Chem. Phys. **100**, 2394 (1994).
[21] A. Franceschetti, H. Fu, L.-W. Wang, and A. Zunger, Phys. Rev. B **60**, 1819 (1999).
[22] M. Califano, A. Franceschetti, and A. Zunger, Phys. Rev. B **75**, 115401 (2007).
[23] S. H. Kan, A. Aharoni, T. Mokari, and U. Banin, Faraday Discuss. **125**, 23 (2004).
[24] O. Millo, D. Steiner, D. Katz, A. Aharoni, S. H. Kan, T. Mokari, and U. Banin, Physica E (Amsterdam) **26**, 1 (2005).
[25] T. Puangmali, M. Califano, and P. Harrison (unpublished).
[26] H. Htoon, J. A. Hollingsworth, R. Dickerson, and V. I. Klimov, Phys. Rev. Lett. **91**, 227401 (2003).
[27] H. Fu, L.-W. Wang, and A. Zunger, Phys. Rev. B **57**, 9971 (1998).
[28] F. A. Reboredo and A. Zunger, Phys. Rev. B **63**, 235314 (2001).
[29] V. A. Singh and L. Kumar, Am. J. Phys. **74**, 412 (2006).
[30] D. J. BenDaniel and C. B. Duke, Phys. Rev. **152**, 683 (1966).
[31] A. Franceschetti and A. Zunger, Phys. Rev. B **62**, 2614 (2000).